Baseline and Projected Future Carbon Storage and Carbon Fluxes in Ecosystems of Hawai‘i
Editors: Paul C. Selmants, Christian P. Giardina, James D. Jacobi, and Zhiliang Zhu
U.S. Geological Survey Professional Paper 1834, 2017

Chapter 8. Projected Future Carbon Storage and Carbon Fluxes in Terrestrial Ecosystems of Hawai‘i from Changes in Climate, Land Use, and Disturbance

By Benjamin M. Sleeter,[1] Jinxun Liu,[1] Colin J. Daniel,[2] Todd J. Hawbaker,[1] Tamara S. Wilson,[1] Lucas B. Fortini,[1] James D. Jacobi,[1] Paul C. Selmants,[1] Christian P. Giardina,[3] Creighton M. Litton,[4] and R. Flint Hughes[3]

8.1. Highlights

- For the State of Hawai‘i, total carbon storage was projected to increase by about 6 percent (14.7 TgC) to 267.6 TgC in 2061.
- Carbon stored in living biomass was projected to decrease by approximately 1.3 percent by 2061, from 52.0 TgC to 51.3 TgC; soil organic carbon was projected to increase from 183.6 TgC to 198.0 TgC.
- Net ecosystem production (NEP) for the State of Hawai‘i was estimated at an average annual rate of 0.799 TgC/yr (mean annual NEP carbon flux density of 49 gC/m^2/yr). When land-use change and disturbances were considered, statewide net ecosystem carbon balance (NECB) was estimated at an average annual rate of 0.595 TgC/yr (mean annual NECB carbon flux density of 36 gC/m^2/yr). Both NEP and NECB were projected to decrease during the 50-year projection period, indicating a reduction in statewide carbon-sink strength. Developed lands were projected to more than double (increasing by ~1,100 km^2) by 2061 and account for 12.2 to 13.7 percent of the State's land area. Conversion to development would account for an average net annual loss of 0.1 TgC/yr.
- Agricultural lands were projected to decrease sharply in the "business as usual" projection, with contraction rates (~45 km^2/yr) more than double the rate of expansion (20 km^2/yr). Agricultural expansion accounted for an average annual loss of 0.078 TgC/yr.
- Wildfire was projected to impact 41 km^2/yr and burn 2,047 km^2 by 2061. Grasslands accounted for 41 percent of all fire, shrublands accounted for 42 percent, and forests accounted for 17 percent. Fire was most common in the dry moisture zone (average of 31 km^2/yr), accounting for 76 percent of the annual burned area.
- Changes involving land-use transitions had the largest impact on total ecosystem carbon storage. Urbanization had the largest negative impact on total ecosystem carbon storage (from 4.0 to 7.4 TgC) and losses of agriculture had the strongest positive impact (from 7.4 to 10.4 TgC). By comparison, wildfire had a relatively small influence.

8.2. Introduction

Human caused changes in land use and land cover (LULC) can alter terrestrial ecosystem carbon stocks and carbon fluxes (Houghton and others, 1999). Since the first human occupants arrived more than 800 years ago, the native, natural landscapes of the Hawaiian Islands have undergone numerous waves of LULC change, from the first Hawaiians' efforts to grow food, fiber, and fuel, to widespread deforestation and introduction of exotic invasive plant species following European contact, to the more recent increase in urbanization. Given Hawai‘i's volcanic composition, carbon-storage potential, and land-use history, it is important to assess the carbon sources and sinks under a range of controlling processes, including ecosystem changes resulting from climate change, wildfire, urbanization, and other anthropogenic drivers (Osher and others, 2003).

The Land Use and Carbon Scenario Simulator (LUCAS) model (Sleeter and others, 2015) was used to project changes in LULC and ecosystem carbon storage and flux under a "business as usual" (BAU) scenario for the State of Hawai‘i. This report describes the model and corresponding parameters (section 8.3), results of the simulations (section 8.4), as well as some of the key uncertainties and limitations of this study (section 8.5).

8.3. Input Data and Methods

The LUCAS model was used to understand how changes in land use and land cover—in particular urbanization, agricultural expansion and contraction, wildfire, and vegetation dynamics—affect carbon storage and fluxes for the State of Hawai‘i. The LUCAS model is an integrated state-and-transition simulation

[1]U.S. Geological Survey.
[2]University of Toronto.
[3]U.S. Department of Agriculture Forest Service.
[4]University of Hawai‘i at Mānoa.

and stock-flow (SF) model, which was linked to the Integrated Biosphere Simulator (IBIS) to provide carbon-flux rates. The LUCAS model produces spatially explicit projections of land change while also tracking the flow of carbon between various pools. See Sleeter and others (2015) for a complete description of the LUCAS model, including the linkage to IBIS. A description of the software and modeling framework used to implement the LUCAS model can be found in Daniel and Frid (2012) and Daniel and others (2016). The ST-SIM software application (ver. 3.0.17) can be downloaded from Apex Resources Management Solutions (http://www.apexrms.com).

8.3.1. State Variables and Scales

The modeling process covers most of the State of Hawai‘i, including the islands of Hawai‘i, Kaho‘olawe, Kaua‘i, Lāna‘i, Maui, Moloka‘i, and O‘ahu. The island of Ni‘ihau was not included in this analysis. Additionally, Hawai‘i was subdivided into three moisture zones—dry, mesic, and wet—and subdivided into 16,146 1 × 1-km simulation cells (fig. 8.1). The temporal resolution of the model was set to annual timesteps.

The primary state variable tracked in the model was the state of each simulation cell. Each cell was assigned to 1 of 189 unique state-class types representing the combination of 3 moisture zones, 7 islands, and 9 LULC classes (forest, grassland, shrubland, tree plantation, developed, agriculture, barren, water, and wetland). In addition to the state of each cell, the LUCAS model tracks the age and the time since transition (TST) of each cell. For this model we tracked the age of forests, grasslands, shrublands, and tree plantations; TST was tracked for fire occurring on the grassland state class. No changes were simulated for water and wetland state-class types.

8.3.2. Process Overview

Transition pathways are defined as the set of changes that can move a cell from one state to another. Transition pathways are defined for all possible conversions simulated within the model. These include transitions associated with urbanization, agricultural expansion, agricultural contraction, wildfire, shrub encroachment, forest management, and changes in the size and spatial distribution of moisture zones under future projections of climate change. Within each timestep the ordering of the transition pathways was conducted randomly. Temporally, transition probabilities can be specified as static or varying. For this model we identified a total of 7 transition groups, 14 transition types, and 107 transition pathways (table 8.1). All transitions were modeled at an annual timestep.

Table 8.1. Transition pathways defined for the Land Use and Carbon Scenario Simulator (LUCAS) model.

[LULC, land use and land cover]

Transition group	Transition type	Number of pathways	From state		To state	
			Moisture zone	LULC class	Moisture zone	LULC class
Agricultural expansion	Agricultural expansion	9	All	Forest, shrubland, grassland	All	Agriculture
Agricultural contraction	Agricultural contraction	9	All	Agriculture	All	Forest, shrubland, grassland
Urbanization	Urbanization	15	All	Forest, shrubland, grassland, agriculture, barren	All	Developed
Management	Forest harvest	3	All	Forest	All	Forest
	Forest plantation	3	All	Forest	All	Plantation
	Plantation harvest	3	All	Plantation	All	Plantation
Vegetation change	Shrub encroachment	2	Dry	Grassland	Dry	Shrubland
			Mesic		Mesic	
Moisture zone change	Dry to mesic	9	Dry	All	Mesic	All
	Mesic to dry	9	Mesic		Dry	
	Mesic to wet	9	Mesic		Wet	
	Wet to mesic	9	Wet		Mesic	
			Wildfire submodel			
Wildfire	High severity	9	All	Forest	All	Grassland
				Shrubland		Grassland
				Grassland		Grassland
	Medium severity	9	All	Forest	All	Forest
				Shrubland		Shrubland
				Grassland		Grassland
	Low severity	9	All	Forest	All	Forest
				Shrubland		Shrubland
				Grassland		Grassland

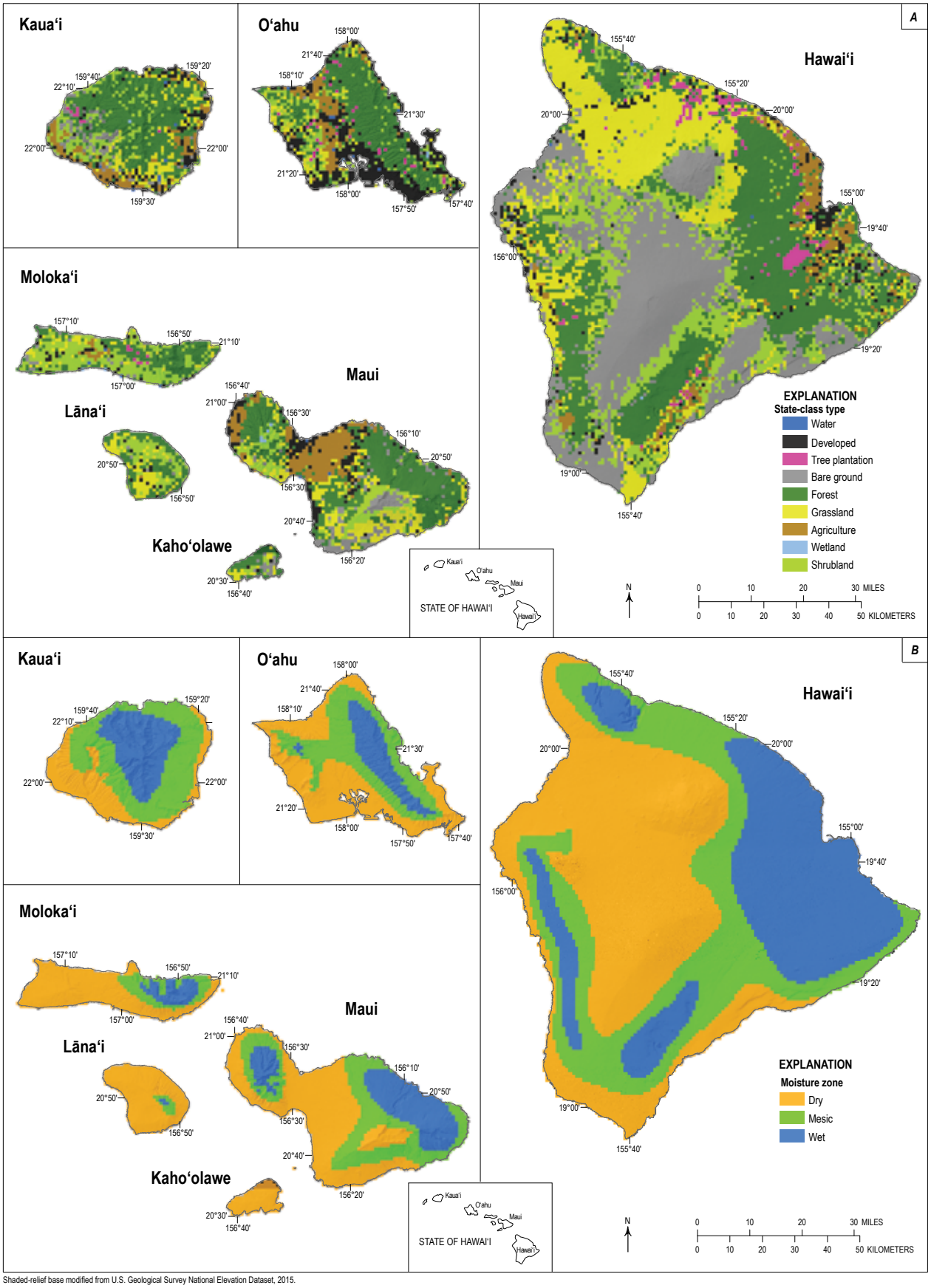

Shaded-relief base modified from U.S. Geological Survey National Elevation Dataset, 2015.

Figure 8.1. Maps showing state-class types (*A*) and moisture zones (*B*) used to initialize the Land Use and Carbon Scenario Simulator (LUCAS) model for Hawai'i.

8.3.3. Model Parameterization

8.3.3.1. Transition Probabilities

Transition targets are used to model changes owing to agricultural expansion, agricultural contraction, urbanization, management, biome change, and moisture-zone change. Transition targets for agricultural expansion, agricultural contraction, and urbanization were based on a time series of change rates from remote-sensing-based mapping by the National Oceanic and Atmospheric Administrations (NOAA) Coastal Change Analysis Program (C-CAP). The C-CAP data provides classified land-cover images for Hawai'i for the years 1992, 2001, 2005, and 2010 (NOAA, 2013). For these four dates and three temporal intervals we calculated the rate for each transition across the entire state. To represent this range of historical variability we sampled from a uniform distribution fitted to the minimum and maximum values from the C-CAP data (table 8.2). Transition targets to model changes in moisture zones were based on projections in Fortini and others (this volume, chap. 3). Maps of moisture-zone changes for the period 2000–2100 were used to calculate an annualized rate of change for each of the moisture-zone conversions. These rates were then applied annually for each timestep within all Monte Carlo simulations of the model (table 8.2). The management transition group consists of three transition types: forest harvest, forest-to-tree plantation conversion, and tree-plantation harvest. Due to a lack of contemporary information, transition targets for forest and tree-plantation management were set to zero under the BAU scenario.

Compared to other transition types, wildland fire transitions were handled uniquely in the model using an approach that initiated wildland fire ignitions and then spread into adjacent pixels. The wildland fire size distribution and transition probabilities were based on the time series of burned area and severity mapped from Landsat imagery between 2002 and 2011 using the Monitoring Trends in Burn Severity (MTBS) project's mapping protocol for fires larger than 0.4 km² (Eidenshink, 2007), as described in Hawbaker and others (this volume, chap. 5). For each timestep and Monte Carlo simulation, the number and size of fires was randomly drawn from the baseline fire size distribution (table 8.3). Fires

Table 8.2. Transition targets and probabilities used in the Land Use and Carbon Scenario Simulator (LUCAS) model for the "business as usual" scenario.

[prob, probability]

Transition type	Moisture zone		From class	To class	Mean area (km²)	Min area (km²)	Max area (km²)	Distribution type
Agricultural expansion	N/A		Forest, shrubland, grassland	Agriculture	---	3	50	Uniform
Agricultural contraction	N/A		Agriculture	Forest, shrubland, grassland	---	25	65	Uniform
Urbanization	N/A		Forest, shrubland, grassland, agriculture, barren	Developed	---	12	32	Uniform
Moisture zone change	Dry	Mesic	All	All	8	---	---	---
	Mesic	Dry			19.42	---	---	---
	Mesic	Wet			7	---	---	---
	Wet	Mesic			3	---	---	---
Transition type	**Moisture zone**		**From class**	**To class**	**Mean prob**	**Min prob**	**Max prob**	**Distribution type**
Shrub encroachment	Dry, mesic, wet		Grassland	Shrubland	---	0.006	0.0327	Uniform

Table 8.3. Transition probabilities for the wildland fire transition type for different moisture zones, state classes, and years.

Year	Forest			Shrubland			Grassland		
	Dry	Mesic	Wet	Dry	Mesic	Wet	Dry	Mesic	Wet
2002	0.0004	0.0010	0.0006	0.0013	0.0053	0.0093	0.0005	0.0029	0.0003
2003	0.0043	0.0030	0.0039	0.0118	0.0162	0.0021	0.0082	0.0087	0.0008
2004	0.0006	0.0000	0.0000	0.0014	0.0000	0.0000	0.0011	0.0000	0.0000
2005	0.0036	0.0000	0.0000	0.0068	0.0002	0.0002	0.0633	0.0000	0.0001
2006	0.0014	0.0000	0.0000	0.0066	0.0000	0.0000	0.0157	0.0014	0.0000
2007	0.0074	0.0038	0.0000	0.0166	0.0027	0.0000	0.0397	0.0005	0.0000
2008	0.0053	0.0003	0.0000	0.0002	0.0018	0.0000	0.0025	0.0058	0.0020
2009	0.0032	0.0001	0.0000	0.0190	0.0017	0.0000	0.0016	0.0000	0.0000
2010	0.0015	0.0001	0.0000	0.0061	0.0003	0.0000	0.0088	0.0005	0.0000
2011	0.0000	0.0011	0.0010	0.0000	0.0025	0.0011	0.0033	0.0001	0.0002

were initiated at randomly selected ignition points in burnable state classes (forest, shrubland, and grassland) and weighted by baseline burn probabilities for each state class (for example, grasslands had higher ignition probabilities than forests). Once initiated, fires would spread to adjacent pixels based on their transition multipliers (table 8.4) until the fire reached its randomly selected fire size or there were no more burnable pixels left to spread into. Fire spread was not adjusted to account for effects of slope or wind speed (daily weather were not used as inputs) as has been done with some other state-and-transition models (STSMs) (Liu and others, 2015); however, this had little effect on the simulated shapes and sizes of fires given the generally small size of fires in Hawai‘i and the 1 × 1-km resolution of cells used in the model. As pixels were burned, they were randomly assigned a burn-severity category based on an additional set of transition multipliers (historical proportions for each state class and burn-severity class; table 8.5). The burn-probability category determined the state-class transition of a pixel (table 8.1). For both ignitions and spread, year-to-year variability was introduced by randomly selecting burn probabilities from one of the baseline years (2002–2011; table 8.4). Using this approach, future potential changes in the amount of area burned by wildland fires were a function of changes in the area of different burnable state classes.

Transition multipliers were also used to project changes in shrub encroachment; however, little is known about the rates of shrub encroachment in Hawai‘i and large uncertainties exists surrounding the rates and pattern of conversion. In the dry and mesic moisture zones, grassland cells that had not experienced fire for 10 years became eligible for shrubland encroachment. For each Monte Carlo simulation, we sampled from a uniform distribution of values representing a 0.95 cumulative transition probability for 50 and 500 years without fire, resulting in annual transition probabilities ranging from 0.0327 to 0.006 (table 8.2).

Table 8.4. Distribution of wildfire sizes (burned area and patch size).

Min area (km^2)	Max area (km^2)	Proportion of events
0	1.0	0.5843
1.1	2.0	0.3983
2.1	5.0	0.1895
5.1	10.0	0.0885
10.1	25.0	0.0243
25.1	50.0	0.0073
50.1	75.0	0.0033
75.1	100.0	0.0018
100.1	200.0	0.0004

8.3.3.2. Spatial Multipliers

Within the model, two types of spatial constraints were used to influence the pattern of LULC transitions. First, adjacency rules were established to drive transitions into cells immediately adjacent to existing cells classified in the “to” state class. For example, transitions into development (urbanization pathway) could only occur in cells immediately adjacent to existing developed cells. Second, spatial layers representing land ownership, protected lands, and land-use zoning were used to prohibit or limit changes from certain cells.

For the agricultural expansion, agricultural contraction, urbanization, and moisture-zone transitions, adjacency settings were established where candidate cells for each transition type were assigned a cell-based probability that was a linear function of the eight neighboring cells classified in the “to” class. The effect of this parameter setting results in cells with a higher number of neighbors being given a higher spatial multiplier value. Cells with no neighbors were assigned a transition multiplier value of zero, resulting in no possibility of transition. For the shrub encroachment transition, all cells with at least one neighbor were assigned values of one and cells with no neighbors were assigned a value of zero. The process for calculating adjacency probabilities was updated every 5 years for all transitions.

In addition to adjacency rules described above, a set of spatial maps was developed to further refine the location of modeled transitions. For the agricultural expansion pathway, a map of areas prioritized for agricultural production was obtained from the State of Hawai‘i Office of Planning (http://planning.hawaii.gov/gis/download-gis-data/). Cells classified as “zoned for agriculture” were assigned a spatial multiplier value of one; all other cells were assigned a value of zero (fig. 8.2). The same dataset was used to restrict urbanization where cells classified as “urban” were assigned a value of one. So as not to entirely limit urbanization from occurring in cells outside this zoned area, all other cells were assigned a spatial multiplier value of 0.5. Lastly, for both transitions, cells designated for conservation were assigned a value of zero, and were not allowed to experience a land-use conversion into agriculture or development (fig. 8.2).

Table 8.5. Burn-severity probabilities for different moisture zones and state classes.

Moisture zone	Forest			Shrubland			Grassland		
	Dry	Mesic	Wet	Dry	Mesic	Wet	Dry	Mesic	Wet
High	0.0087	0.1207	0.0052	0.0047	0.0637	0.0348	0.0150	0.0109	0.0056
Medium	0.0826	0.3324	0.3452	0.1325	0.3910	0.6902	0.1074	0.1620	0.2767
Low	0.9086	0.5469	0.6496	0.8629	0.5454	0.2750	0.8801	0.8271	0.7178

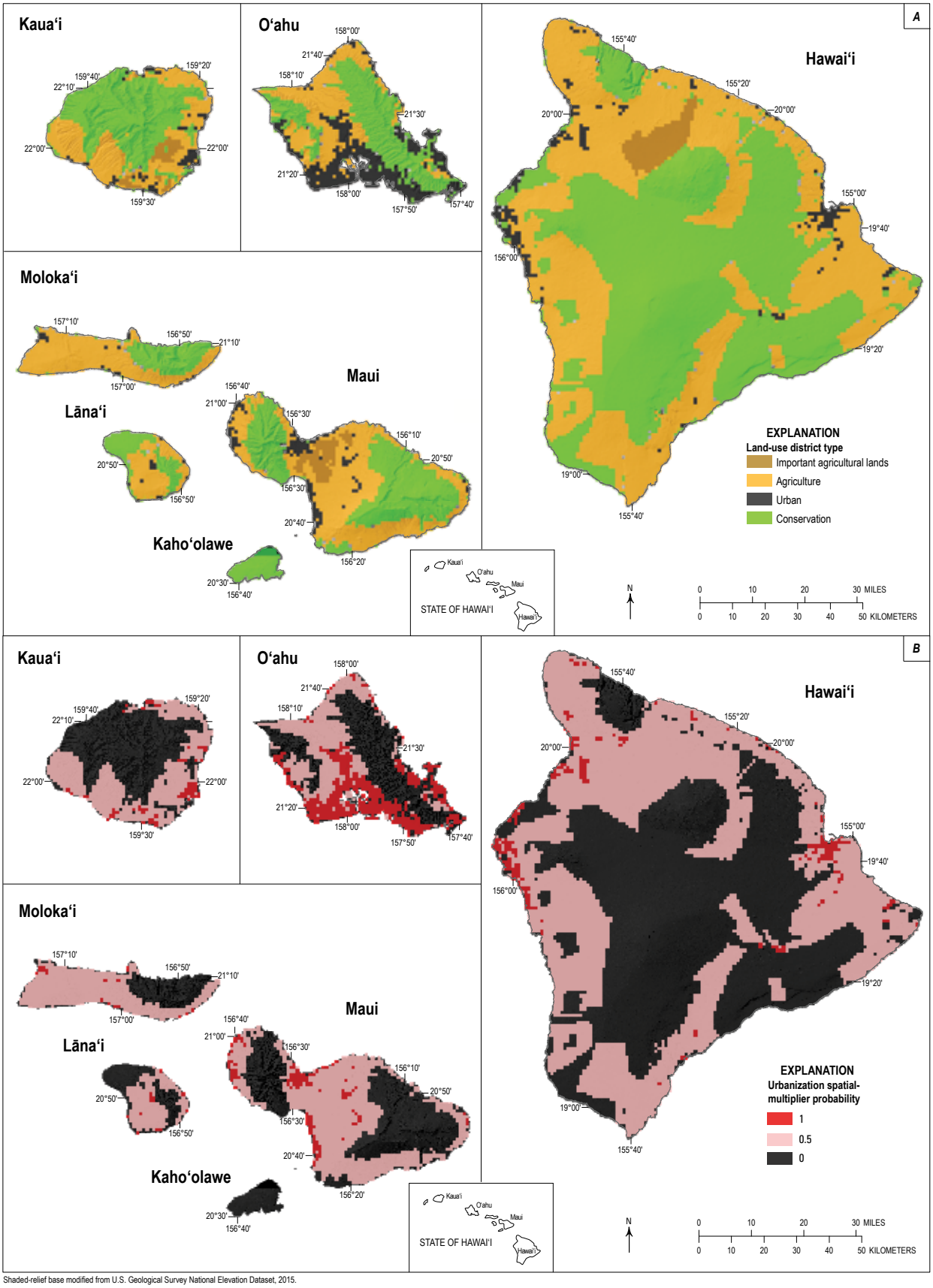

Shaded-relief base modified from U.S. Geological Survey National Elevation Dataset, 2015.

Figure 8.2. Maps showing State of Hawai'i Land-Use Districts which were used to generate spatial multiplier probabilities. *A*, Original source data. *B*, Urbanization spatial multiplier. *C*, Agricultural-expansion spatial multiplier (facing page).

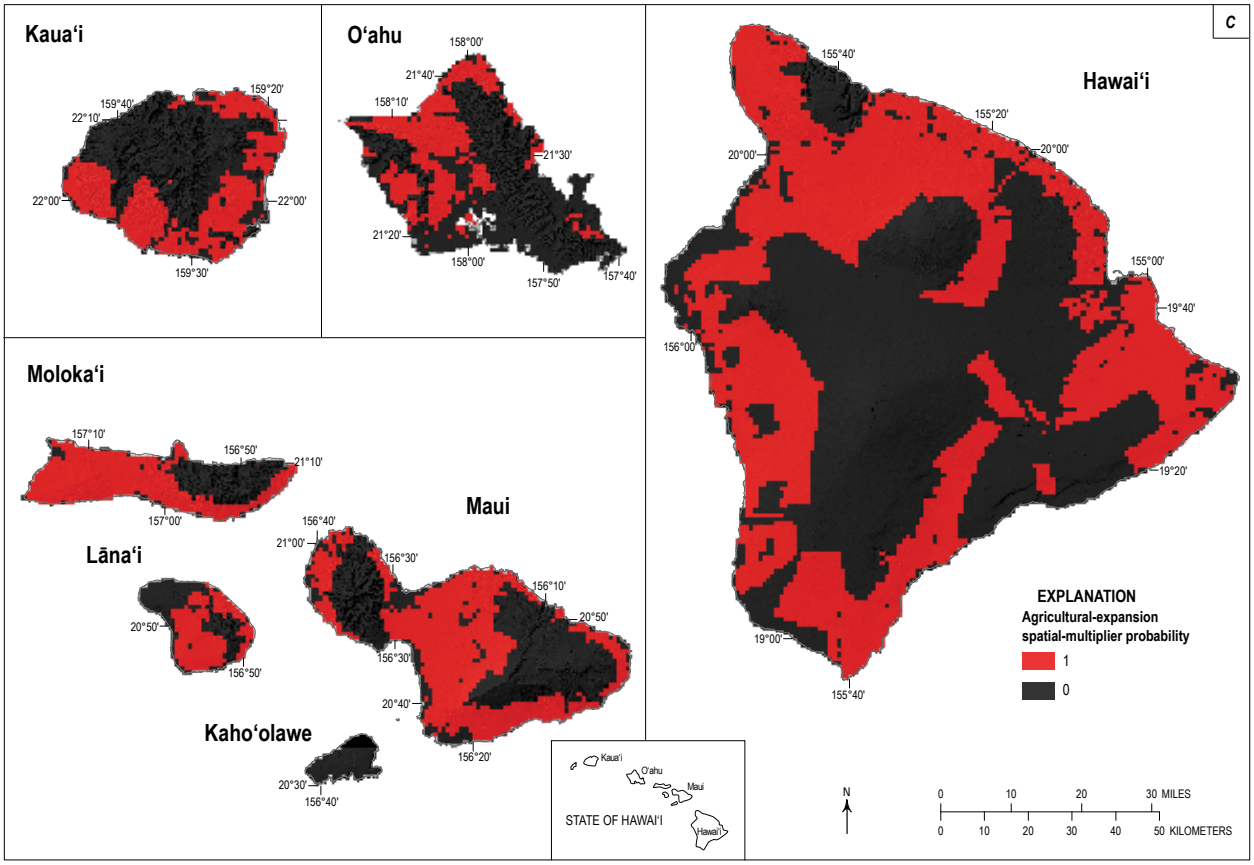

Shaded-relief base modified from U.S. Geological Survey National Elevation Dataset, 2015.

Figure 8.2.—Continued

Agricultural contraction was allowed to occur on all lands with the exception of "high priority agricultural lands" as classified by State of Hawai‘i Office of Planning (http://planning.hawaii.gov/gis/download-gis-data/); all cells within these areas were given a value of zero, whereas all other cells were allowed to transition out of agriculture. These areas were generally confined to Waimea on the Island of Hawai‘i, Maui's Central Valley, and near Lihue on Kaua‘i (fig. 8.2).

Changes in the spatial extent of moisture zones were limited to areas projected in Fortini and others (this volume, chap. 3). Maps of changes between dry, mesic, and wet moisture zones were obtained for the 2000–2100 period; cells where changes in moisture zone were projected to occur were assigned a value of one, whereas all other cells were assigned a value of zero.

8.3.4. Model Initialization

Each cell was assigned to 1 of 210 unique state classes based on the spatial intersection of moisture zones (Fortini and others, this volume, chap. 3), islands, and a map of LULC (Jacobi and others, this volume, chap. 2). The moisture-zone map was resampled to 1-km resolution using a nearest-neighbor algorithm (fig. 8.1). To estimate the initial LULC for each cell, the carbon assessment for Hawai‘i (CAH) land-cover map was first reclassified from its original 27 classes to match the classification scheme described in section 8.3.1. Next, the reclassified LULC map was resampled from its original 30-m resolution to 1-km cells using a majority algorithm (fig. 8.1). The origin and projection of both the moisture-zone and LULC map were set to match each other using a Universal Transverse Mercator Projection (UTM zone 3, NAD83 datum). Lastly, a map of the State of Hawai‘i was obtained from the State of Hawai‘i Office of Planning (http://planning.hawaii.gov/gis/download-gis-data/) and resampled to match the spatial parameters of the other two maps. The three spatial maps were then overlaid and each cell was assigned to one of the 210 unique combinations of moisture zone, island, and LULC class, resulting in the initial state-class map. The same initial conditions were used for all Monte Carlo simulations.

Age was tracked as a state-class variable for forests, shrublands, grasslands, and tree plantations; however, there are no known data describing the present-day age distribution of Hawai‘i ecosystems. For forests, shrublands, and grasslands, age was randomly assigned to each cell from a uniform distribution between 0 and 300. For tree plantations, we assumed a uniform distribution of ages between 0 and 50. Initialization of time-since-transition was tracked for wildfire for the grasslands class. To initialize TST we assumed a uniform distribution of values between 0 and the average fire-return interval for grasslands within each moisture zone—69 years for dry grasslands and 502 years for mesic grasslands.

8.3.5. Carbon Accounting Submodel

The carbon accounting submodel was designed to track the stocks and fluxes of carbon over time resulting from natural ecological processes (for example, growth or mortality) and changes in LULC, which can be functions of a change in climate (moisture-zone shifts), wildfire, and other anthropogenic drivers. The methods used to parameterize and run the integrated carbon submodel are based on Sleeter and others (2015), and follow a general SF or systems-dynamics approach and a tier 3 approach to carbon accounting, which requires locally specific, high-quality input data, recommended by the Intergovernmental Panel on Climate Change (IPCC, 2006). We use the term "flow pathways" to define the movement of carbon from one stock to another (for example, carbon flux). Flow pathways can occur automatically (for example, growth of biomass), or be related to transitions modeled in the STSM (for example, wildfire resulting in the flux of carbon from biomass to the atmosphere or deadwood pools). The SF model tracks the stock and flow of carbon across forest, grassland, shrubland, and tree-plantation state-class types. For all other state classes we assume carbon stocks are stable.

The SF submodel tracks carbon stored in the following pools: living biomass, litter, standing deadwood, downed deadwood, and soil. In addition, the model tracks carbon moved to the atmosphere by emissions, soil leaching from aquatic systems, and harvested wood products. Carbon is tracked on an annual timestep for each Monte Carlo simulation in forest, shrubland, grassland, and tree-plantation classes. Flow pathways include growth, litterfall, humification, emission, mortality, and harvest (table 8.6). Depending upon the flow type, the rate at which carbon is moved from one pool to another may vary based on state-class type, age, timestep, and (or) Monte Carlo simulation. Furthermore, flows of carbon between stock types are divided between "automatic" and "event-based" flows, where automatic flows occur for all cells in all timesteps, and event-based flows only apply to cells that experience a state transition (Sleeter and others, 2015). For each timestep and Monte Carlo simulation, the order of flows was implemented at random.

We used the IBIS model to generate automatic flow rates for forest, shrubland, and grassland state classes. IBIS (Foley and others, 1996; Kucharik and others, 2000) is a modeling framework that follows basic rules of physics, plant physiology, and biogeochemistry. The original model combined features of a mechanistic model of canopy photosynthesis (Farquhar and others, 1980), a semi-mechanistic model of stomatal conductance (Ball and others, 1987), an algorithm on phenology (Botta and others, 2000), and several soil biogeochemical models (Parton and others, 1987, 1993; Verberne and others, 1990) in a single application. IBIS has the ability to simulate major land-surface processes, canopy physiology, vegetation phenology, long-term vegetation dynamics, ecosystem production, and carbon cycling.

The approach to developing automatic flow rates was based on methods developed by Sleeter and others (2015) which link the IBIS model to the SF submodel described here. A calibration simulation was run in IBIS using "cold start" procedures, which supply the SF submodel with automatic flow pathway rates. The IBIS cold-start simulation starts with bare ground for all cells and then simulates the growth of vegetation in response to average historical climate conditions for the region. To calibrate IBIS to local conditions we used estimates of net primary production (NPP) derived from gross primary production (GPP) from Selmants and others (this volume, chap. 6) and aboveground living biomass described in Selmants and others (this volume, chap. 6). A series of IBIS model simulations were run until NPP and living biomass pools were stabilized at levels similar to observed conditions. Carbon flux rates from IBIS (in other words, automatic flows) were generated on annual timesteps and aggregated to the following age categories for the SF submodel: 0–10 years, 10–20 years, 20–50 years, 50–100 years, and greater than 100 years old. All flow pathways were non-time varying, meaning no assumption was made as to how carbon fluxes may change under future conditions. The result of this assumption is, for example, that the rate of forest litterfall for a 50-year-old forest is not changed in future projection years.

The growth flow pathway moves carbon from the atmosphere to living biomass stock and is expressed as NPP. NPP was derived from MODIS GPP estimates described in Selmants and others (this volume, chap. 6). MODIS estimates of NPP are typically derived by modeling components of autotrophic respiration (R_a) and then subtracting R_a from GPP to yield estimates of NPP. However, the BIOME-BGC model of R_a requires the MOD15 leaf area index (LAI) product as an input, which is in part based on the MOD12Q1 land-cover product, and it was not possible to substitute our modified land-cover map into the MOD15 estimate of LAI. Here, NPP was estimated by calculating carbon-use efficiency (CUE; the quotient of NPP divided by GPP) for all pixels from the "off the shelf" 1-km-resolution MOD17 product with land-cover classes that corresponded with those of the land-cover map described in Jacobi and others (this volume, chap. 2), for the period 2002–2010. We then calculated the median CUE for each land-cover type used in this report (table 8.7) and multiplied the modified MOD17 estimates of GPP from Selmants and others (this volume, chap. 6) by these land-cover-specific CUE values to yield a statewide 500-m-resolution layer of terrestrial NPP. The statewide MODIS-derived estimates of NPP were used to calibrate the IBIS model simulation. Within the LUCAS SF submodel, the growth flow pathway was based on IBIS estimates of NPP for each state class and moisture zone combination. IBIS NPP estimates include the annual growth of biomass in aboveground and belowground vegetation, including roots, leaves, and wood. Owing to a lack of future projections of NPP under alternative climate scenarios, annual projections of growth for the SF submodel were derived from the IBIS-modeled mean NPP estimate and allowed to vary by ±5 percent annually.

Seven flow types (growth, litterfall, humification, mortality, deadfall, emissions, and leaching) were specified in the model for each combination of moisture zone, state class, and age class. The tree-plantation class was assigned flow rates from the wet forest state-class type. Growth is the annual rate of carbon accumulation in living biomass expressed as NPP. Litterfall is an

Table 8.6. Carbon-flow types used within the Land Use and Carbon Scenario Simulator (LUCAS) model.
[HWP, harvested wood products]

Carbon-flow type	State class type	Flow pathway type	From stock	To stock
Growth	All	Automatic	Atmosphere	Living biomass
Litterfall	All	Automatic	Living biomass	Litter
	Forest Shrubland Plantation	Automatic	Down deadwood	
Humification	All	Automatic	Litter	Soil
Mortality	Forest Shrubland Plantation	Both	Living biomass	Standing deadwood
Deadfall	Forest Shrubland Plantation	Automatic	Standing deadwood	Down deadwood
Emission	All	Both	Living biomass	Atmosphere
	All		Litter	
	All		Soil	
	HWP	Automatic	Atmosphere	
Harvest	Forest Plantation	Event	Living biomass	HWP

annual flux rate that includes leaf and root biomass moving from the living biomass to the litter stock. Humification is the annual decomposition rate of organic material from litter to soil organic matter. Mortality is an annual rate resulting from natural death of vegetation that also includes mortality resulting from land-use activities such as urbanization, wildfire, and harvest. Deadfall is the annual rate of transfer of carbon between standing and downed deadwood stocks. Emissions include the annual rate of respiration from litter and soil pools (heterotrophic respiration [R_h]) as well as emissions resulting from land-use change and disturbances. Leaching is the annual rate of carbon flux from the soil pool to the aquatic pool. Harvest is the rate of transfer of carbon from the living biomass pool to harvested wood products as a result of land use and land-use change.

Event-based flows are associated with transition pathways from the STSM. When the STSM applies a transition for a given cell the SF submodel applies a predefined set of additional flows to move carbon between stocks. In this model, event-based flows are specified for urbanization, agricultural expansion, and forest and tree-plantation harvest and associated with emission and harvest-flow types. When one of these transitions occurs on a cell, one or more flow pathways are invoked to move carbon between various stocks.

Carbon initial conditions were specified for the living-biomass, soil, litter, standing-deadwood, and downed-deadwood stocks. The model was initialized to match, as closely as possible, estimates of living biomass for each state-class type, based on known reference data described in Hawbaker and others (this volume, chap. 5) and Selmants and others (this volume, chap. 6). Estimates of soil organic carbon were derived from the U.S. Department of Agriculture gridded Soil Survey Geographic (gSSURGO) Database (Soil Survey Staff, 2015; see Selmants and others, this volume, chap. 6). For each combination of state class and moisture zone a mean carbon estimate was derived from the gSSURGO map to initialize the SF submodel. IBIS was used to derive initial estimates for living-biomass, litter, and both standing- and downed-deadwood stocks and calibrated using carbon stock data from Hawbaker and others (this volume, chap. 5). For living biomass on forests and tree plantations, IBIS estimates (which include aboveground and belowground carbon) were compared to estimates of aboveground biomass based on the light detection and ranging (lidar)-derived reference map and the estimates of belowground biomass based on the power law equation described in Selmants and others (this volume, chap. 6).

8.3.6. Simulation Experiments

The model described above was used to project changes in ecosystem carbon under a BAU scenario where landscape changes were a function of the transition pathways and parameters described in section 8.3.3. For the BAU scenario we simulated changes in LULC and carbon during a 60-year projection period spanning the years 2001 through 2061 with

Table 8.7. Estimated carbon-use efficiency for MOD12Q1 biomes used to calculate net primary production.
[Based on the quotient of net primary production divided by gross primary production from 1-km-resolution MOD17 product. CUE, carbon-use efficiency]

MOD12Q1 biome	Median CUE
Broadleaf evergreen forest	0.495
Woody savanna	0.475
Closed shrub	0.545
Open shrub	0.484
Grassland	0.485

the first 10 years being used for model spin-up. During this spin-up period the landscape was fixed and no changes were allowed to occur. Monte Carlo replications of the model were run 100 times to reflect uncertainties in the projection of various state-class transitions. To evaluate impacts of major controlling processes on ecosystem carbon we conducted a series of sensitivity tests to analyze the impact of specific model parameters. Twenty Monte Carlo iterations were run for each of these scenarios.

8.4. Results and Discussion

8.4.1. Projections of Land-Use and Land-Cover Composition and Transitions

Four state classes composed 86.3 percent of Hawai‘i’s land area in 2011: forest (33.8 percent), barren (19.1 percent), grassland (17.0 percent), and shrubland (16.4 percent). Agriculture (5.7 percent) and developed (6.2 percent) land uses accounted for most of the remaining land area. By 2061, the area collectively covered by the four main land-cover classes was projected to decrease slightly to 84.3 percent, however, composition among the four classes changed considerably (fig. 8.4). Forest area decreased to 32.7 percent and barren lands decreased to 18.6 percent of the State’s land area. The most significant changes were between shrubland and grassland composition; grassland area decreased to 10.2 percent, whereas shrubland increased to 22.8 percent. Total land in agriculture decreased sharply to less than 1.0 percent of the State’s area, whereas developed land nearly doubled to 12.9 percent.

The agriculture class was projected to experience the largest loss of any state class, decreasing to less than 180 km^2 by 2061, a net loss of 81.3 percent (fig. 8.3). Nearly all losses in agriculture were through conversion to forests, shrublands, or grasslands; losses to development averaged approximately 2 km^2/yr (fig. 8.4). For the first 30 years of the projection, agricultural contraction (~45 km^2/yr) occurred at a rate more than two times greater than agricultural expansion (~20 km^2/yr) (fig. 8.4). However, by 2045, the rate of contraction was about equal to the expansion rate. Figure 8.5*A* shows the spatial location of where agricultural expansion was most common.

Under the BAU scenario, developed lands were projected to increase by an average of 1,094 km^2 during the 50-year projection period, representing an increase of 107.7 percent over initial conditions (fig. 8.3). By 2061, development was projected to account for between 12.4 and 13.5 percent of the state land area. State classes converted to development were forests (9 km^2/yr), grasslands (5 km^2/yr), and shrublands (5 km^2/yr); barren lands accounted for 2 km^2/yr. For the first 20 years of the projection period, agricultural lands were also contributors to urbanization; however, as agriculture is projected to decrease in area over time, its urbanization becomes minimal. Figure 8.5*B* shows the average annual transition probability for urbanization across 50 years and 100 Monte Carlo iterations.

The major driver of change within the three forest classes was the projected change in moisture-zone composition (see Fortini and others, this volume, chap. 3) (fig. 8.4). Overall, forest area was projected to decrease by 3.4 percent (170 km^2) compared to 2011; however, change was not consistent across moisture zones. Dry forests were projected to increase 33.4 percent (274 km^2), mesic forests were projected to decrease 29.6 percent (1,760 km^2), and wet forests were projected to increase 1.2 percent (11 km^2) by 2061 (fig. 8.6).

Woody encroachment was the only change between vegetation types considered in the model, which resulted in changes from grasslands to shrublands. Across the dry and mesic moisture zones we estimated an average of 1,325 km^2 of grasslands would be converted to shrublands during the 50-year projection. However, there was considerable uncertainty in this projection with estimates ranging from a low of 338 km^2 to a high of 2,265 km^2 (fig. 8.4). Shrublands were projected to increase by 39.2 percent (1,058 km^2), which was ubiquitous across all three moisture zones: dry shrublands increased from 1,422 to 2,096 km^2, mesic shrublands increased from 897 to 1,223 km^2, and wet shrublands increased from 382 to 440 km^2 (fig. 8.6). The area of grasslands decreased in both the dry and mesic moisture zones (from 1,492 to 823 km^2 and from 1,052 to 512 km^2, respectively) and remained relatively stable in the wet moisture zone (fig. 8.6).

Across all state classes and moisture zones, wildfire was projected to burn an average of 41 km^2/yr and a total of 2,047 km^2 by 2061 (fig. 8.4). Grasslands accounted for 41 percent of all wildfire projection, whereas shrublands accounted for 42 percent and forests accounted for 17 percent. Fire was projected to be most common in the dry moisture zone (average of 31 km^2/yr), accounting for 6 percent of the annual area burned. The mesic moisture zone accounted for 17 percent (7 km^2/yr), whereas the wet moisture zone accounted for 6 percent (3 km^2/yr). Low-severity fire accounted for 81 percent of all projected fire (33 km^2/yr), whereas medium-severity fire accounted for 17 percent (7 km^2/yr). High-severity fires accounted for 2 percent of all fire (<1 km^2/yr). The projected annual rates of fire across state classes, moisture zones, and severity classes are shown in figure 8.7.

8.4.2. Projected Change in Total Ecosystem Carbon Storage

Carbon fluxes were modeled for the seven main Hawaiian Islands (excluding Ni‘ihau) and for the forest, shrubland, grassland, and tree-plantation state classes. For state and island totals, stock estimates include carbon stored in soils across all state-class types. Overall estimates of living biomass, litter, and deadwood stocks were developed for only the four state classes where fluxes were modeled.

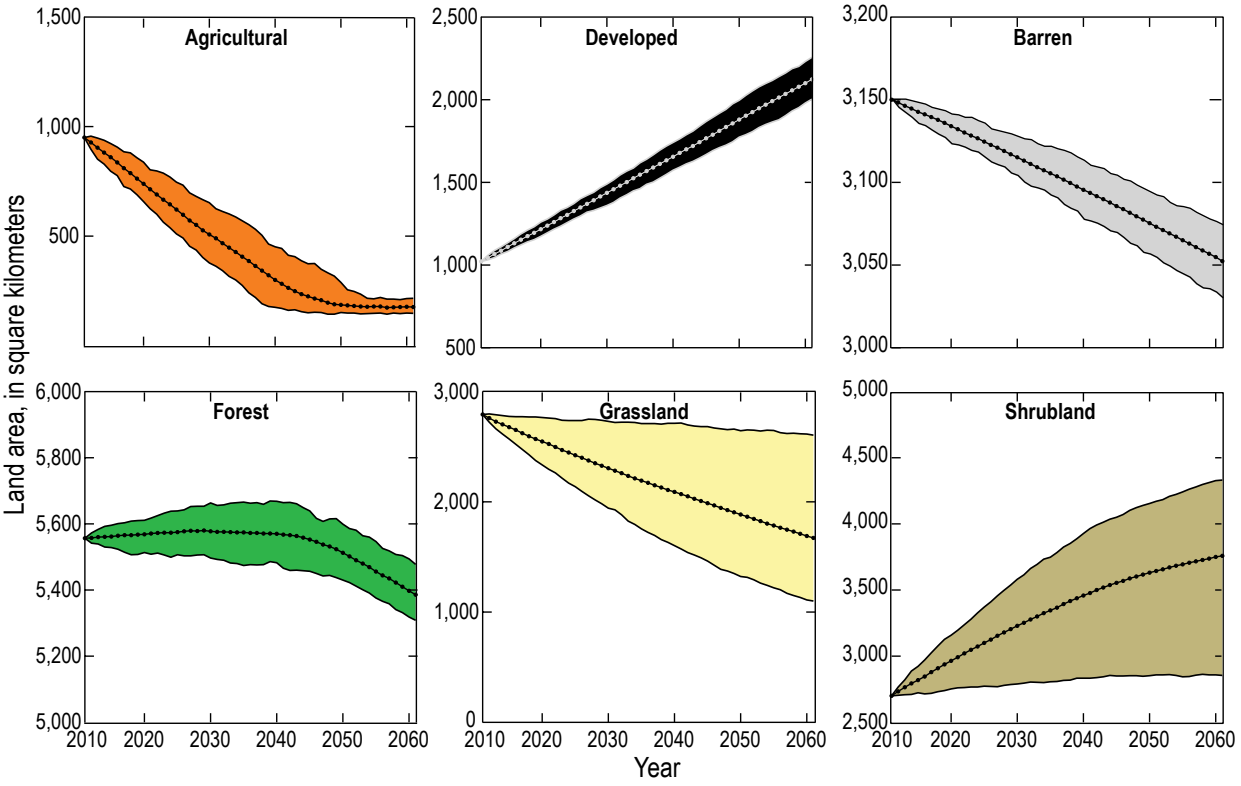

Figure 8.3. Plots of projections of state-class area for the 2011–2061 projection period. The range of values represents the 95-percent confidence interval for each state class across 100 Monte Carlo simulations. Dotted black lines show the mean estimates.

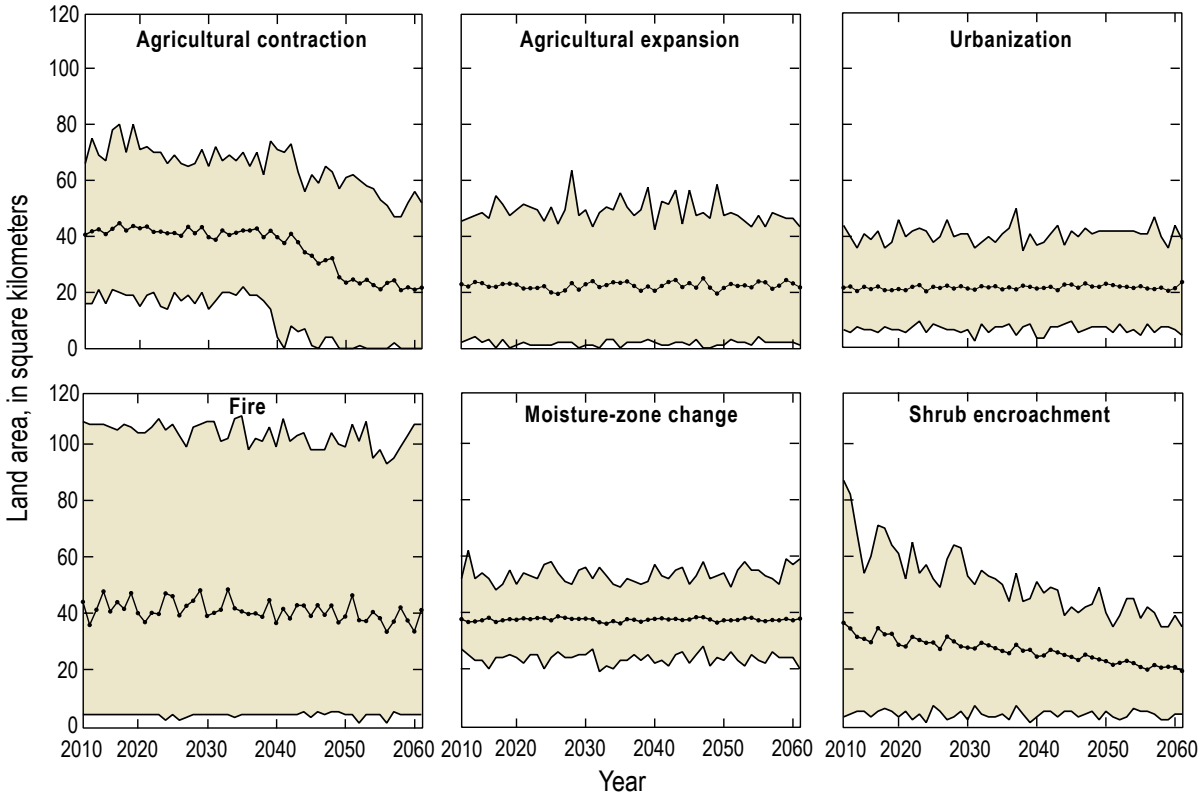

Figure 8.4. Plots of projections of transition groups for the 2012–2061 projection period. The range of values represents the 95-percent confidence interval across 100 Monte Carlo simulations. Dotted black lines show the mean estimates.

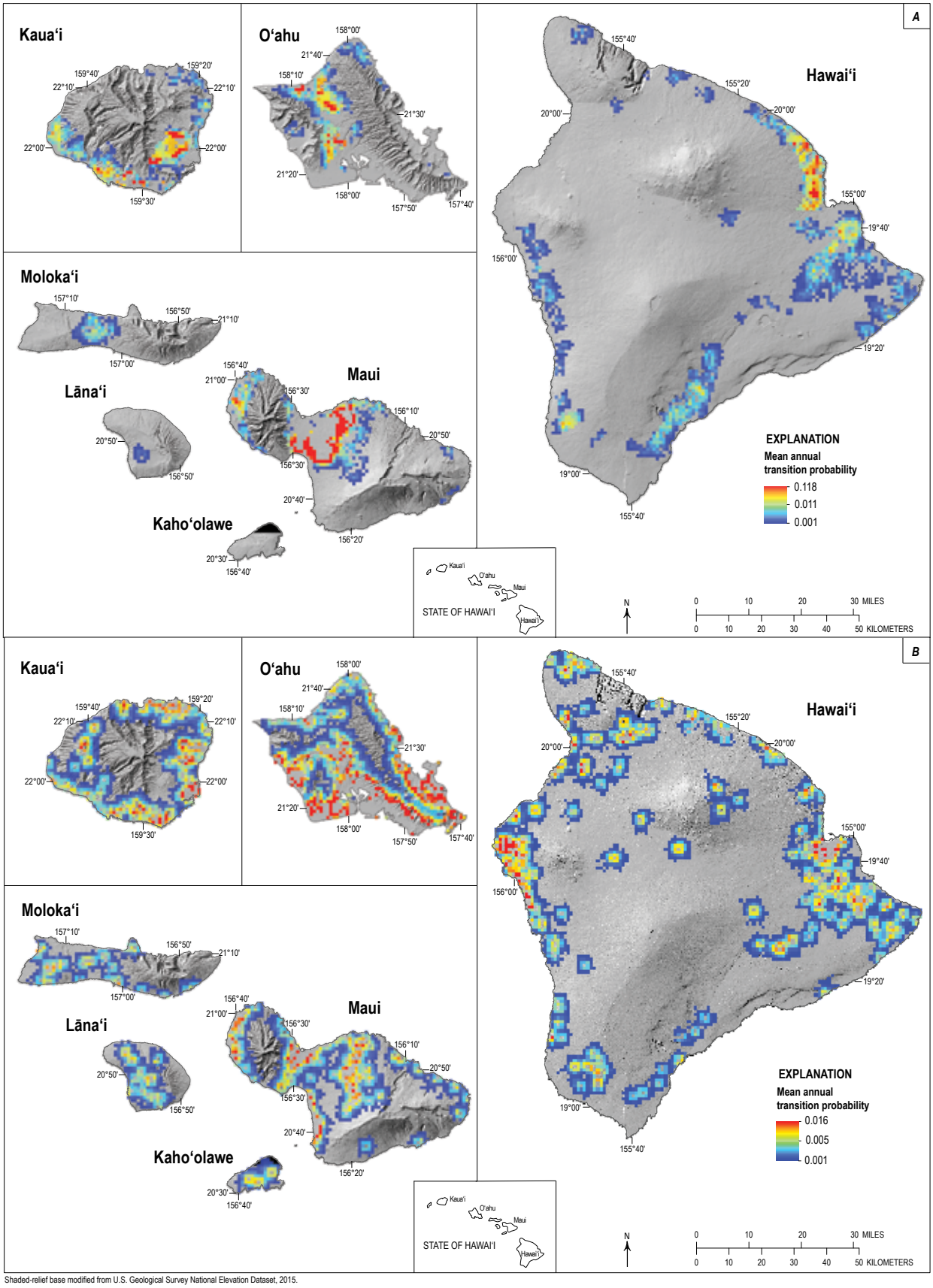

Shaded-relief base modified from U.S. Geological Survey National Elevation Dataset, 2015.

Figure 8.5. Maps showing average annual transition probability across 50 timesteps and 100 Monte Carlo iterations for agricultural expansion (*A*), urbanization (*B*), shrub encroachment (*C*), and wildfire (*D*) in Hawai‘i.

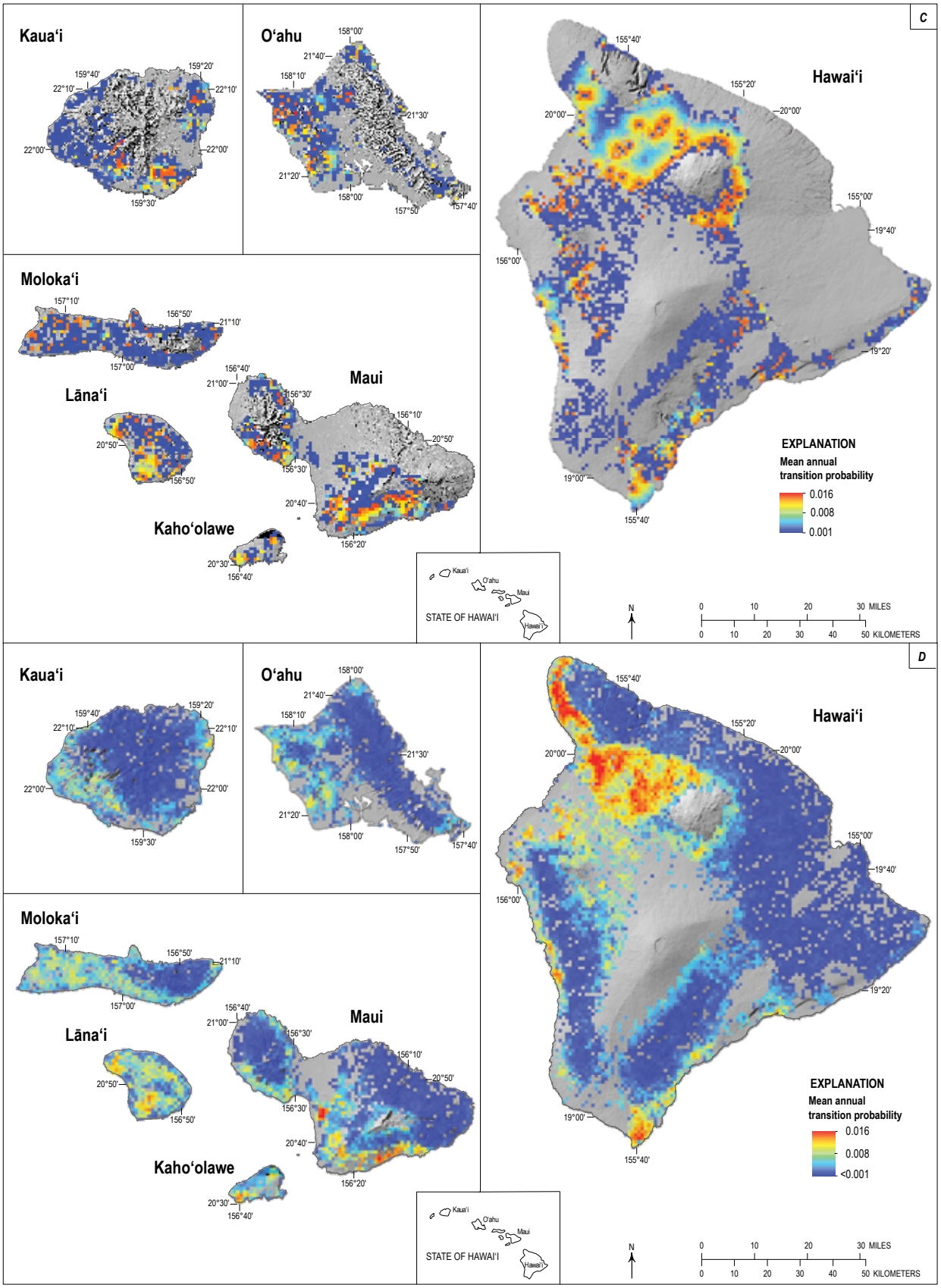

Shaded-relief base modified from U.S. Geological Survey National Elevation Dataset, 2015.

Figure 8.5.—Continued

Initial IBIS-derived estimates of statewide total ecosystem carbon were about 2 percent lower than statewide estimates described in Selmants and others (this volume, chap. 6). Total ecosystem carbon was estimated to increase from 252.9 TgC in 2011 to 267.6 TgC by 2061, a net increase of 14.7 TgC. Carbon stock density for the state was estimated at 15.5 kgC/m^2 and was projected to remain relatively stable throughout the projection period. In 2011, the highest carbon stock densities were found on Kaua‘i (19.6 kgC/m^2), O‘ahu (17.6 kgC/m^2), and Maui (16.6 kgC/m^2). By 2061, total ecosystem carbon storage was projected to increase on six of the major islands and remain relatively stable on O‘ahu (table 8.8). Hawai‘i Island stored the most carbon (its land area accounts for more than half the State's area) at 153.7 TgC in 2011 and was estimated to increase approximately 7.7 percent by 2061 (165.5 TgC).

Total carbon stored in the dry moisture zone was estimated to increase by 37.5 percent, from 46.1 TgC in 2011 to 63.4 TgC in 2061. In the mesic moisture zone, total ecosystem carbon was projected to decrease by 17.6 percent, from 89.7 TgC to 73.9 TgC. Total ecosystem carbon storage in the wet moisture zone was projected to increase 11.3 percent, from 117.0 TgC to 132.3 TgC.

Tables 8.9 and 8.10 show carbon stock estimates for each island and land-cover class, respectively. Similar to results from Selmants and others (this volume, chap. 6), soils

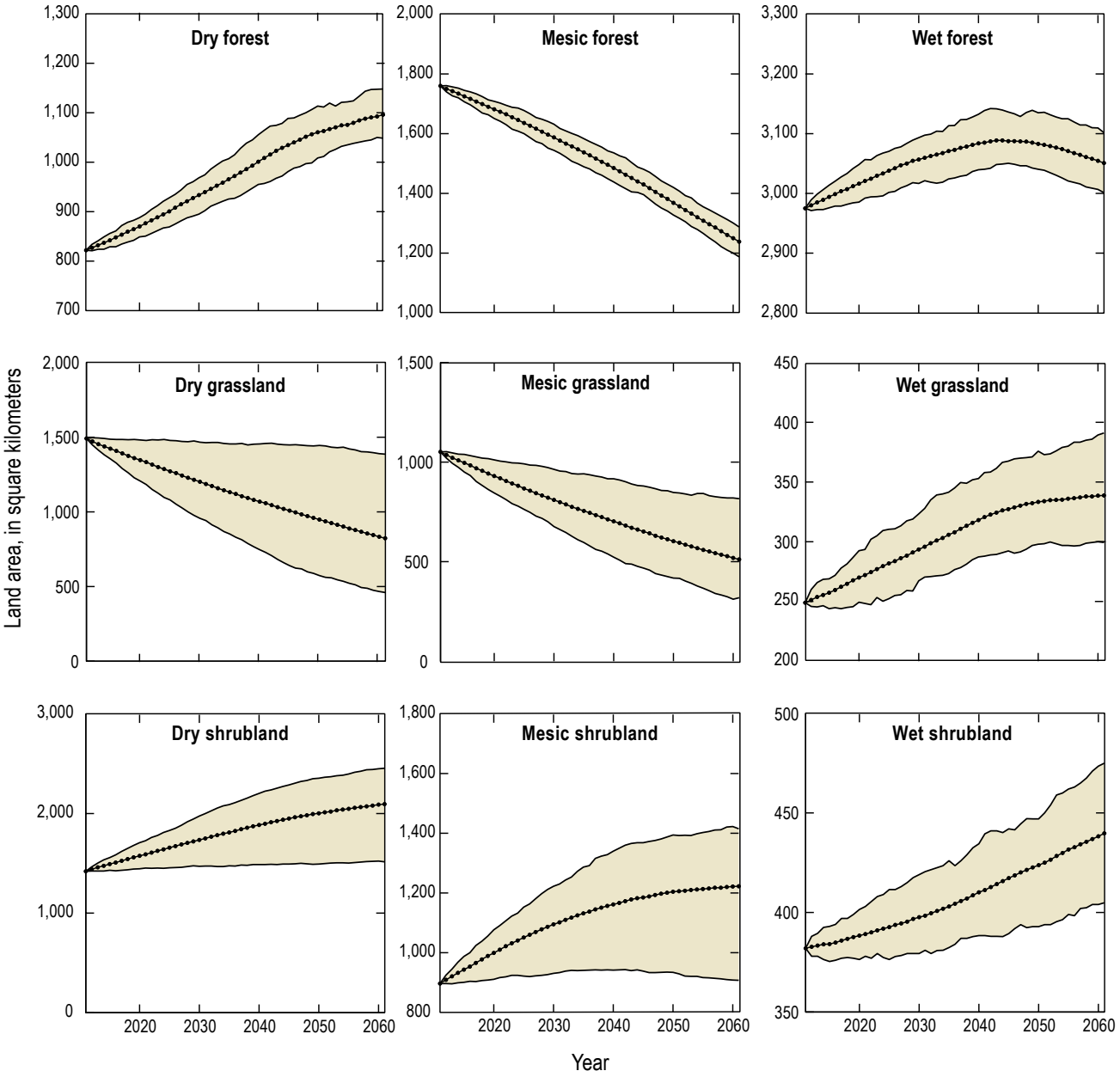

Figure 8.6. Plots of projections of forest, shrubland, and grassland state-class types across the dry, mesic, and wet moisture zones. The range of values represents the 95-percent confidence interval across 100 Monte Carlo simulations. Dotted black lines show the mean estimates.

accounted for approximately 69 percent of carbon stored in terrestrial ecosystems, living biomass accounted for 24 percent, and litter and deadwood stocks accounted for 8 percent; these proportions remained relatively stable during the 50-year projection period. Total living biomass was estimated at 52.0 TgC in 2011 and decreased to 51.3 TgC by 2061. Litter and deadwood was estimated at 27.9 TgC in 2011 and increased 5 percent by 2061 to 29.4 TgC. Carbon stored in soils, across all state classes, was estimated at 183.6 TgC in 2011 and increased 4 percent by 2061 to 198.0 TgC.

In 2011, carbon stored in living biomass was estimated at 52.0 TgC. By 2061, living biomass was estimated to hold 51.3 TgC, a decrease of approximately 1.4 percent during the 50-year projection. Across all moisture zones, forests accounted for the vast majority of living biomass carbon (83 percent), whereas tree plantations (9 percent), shrublands (7 percent), and grasslands (1 percent) accounted for the remainder. Projections of living biomass carbon across moisture zones varied considerably, owing largely to changes in land use, wildfire, shrub encroachment, and moisture-zone extent. The wet moisture zone remained relatively stable during the projection period, increasing by 2.3 TgC from 2011 levels. Conversely, the mesic zone was projected to experience sharp decreases, from 20.1 TgC in 2011 to 15.5 TgC in 2061. Living biomass in the dry moisture zone was projected to increase from 2.9 TgC in 2011 to 4.4 TgC in 2061.

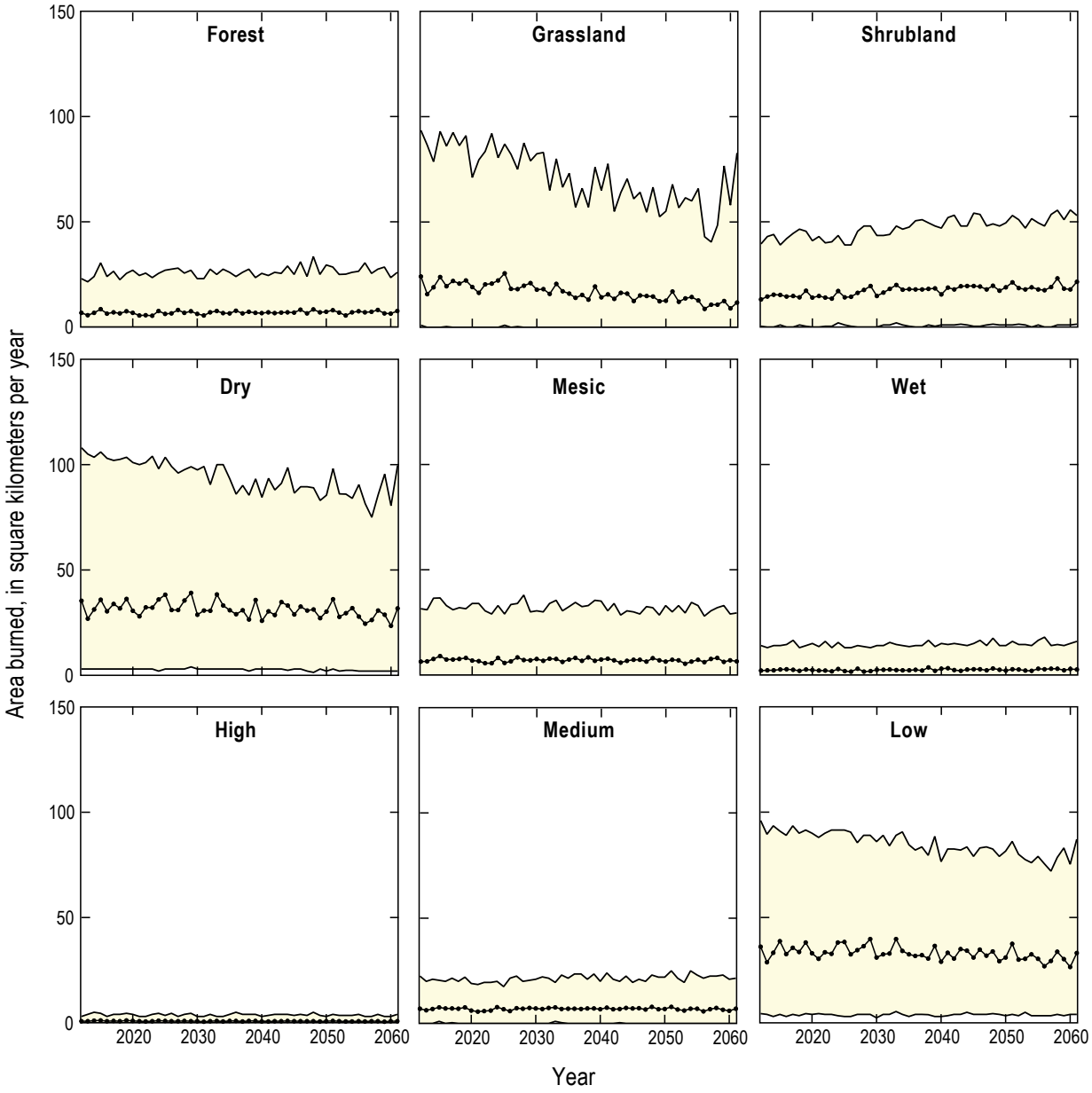

Figure 8.7. Plots of projections of fire by state class, moisture zone, and burn severity during the 2011–2061 projection period. The range of values represents the 95-percent confidence intervals of area burned across 100 Monte Carlo simulations. Dotted black lines show the mean estimates.

Soil organic carbon was estimated to increase from 183.6 TgC to 198.0 TgC between 2011 and 2061. However, when considering only carbon stored in the four state-class types where carbon fluxes were modeled (forest, shrubland, grassland, and tree plantation), soil organic carbon was estimated to increase from 151.7 TgC to 164.8 TgC in 2061. Wet forests stored more than three times the amount of carbon than any other state-class type (65.7 TgC in 2061), followed by Mesic forests which stored 20.9 TgC. Tables 8.9 and 8.10 show the projected change in carbon stocks (by living biomass, soil, and litter and deadwood) between 2011 and 2061 for each island and land-cover class.

8.4.3. Projected Carbon Fluxes

Net ecosystem production (NEP) and net ecosystem carbon balance (NECB) are estimated for the State of Hawai'i and for each of the four state-class types considered in this assessment (forest, shrubland, grassland, and tree plantation). NEP is calculated as the sum of annual growth (NPP) minus R_h from litter and soil pools. NECB is calculated as NEP minus emissions from land-use change and disturbance. Due to constant changes in the state-class (and moisture-zone) area, NEP and NECB estimates are presented as totals (in kilotons of carbon [ktC]).

NEP for the State of Hawai'i was estimated at an average annual rate of 0.799 TgC/yr (49 gC/m^2/yr). When land-use change and disturbances were considered, NECB was estimated at an average annual rate of 0.595 TgC/yr (36 gC/m^2/yr). Both NEP and NECB were projected to decrease during the 50-year projection period indicating the strength of the carbon sink was decreasing. Forest NEP was projected to decrease steadily during the projection period, from approximately 0.754 TgC/yr in 2015 to 0.549 TgC/yr in 2061. Forests in Hawai'i were projected to be a consistent, yet decreasing net sink of carbon, with a mean NECB estimate of 0.481 TgC/yr. However, the strength of the sink was projected to weaken towards the last half of the simulation period. Shrubland NEP was estimated at 0.091 TgC/yr and grasslands were estimated at 0.050 TgC/yr. When considering the effects of land-use change and wildfire, shrublands were a net sink of carbon at a rate of 0.066 TgC/yr, whereas grasslands were a weaker net sink at approximately 0.024 TgC/yr. Figure 8.8 shows estimates of NEP and NECB for each combination of state class and moisture zone.

8.4.3.1. Carbon Losses From Land-Use Change and Wildfire

Urbanization of forests, shrublands, and grasslands resulted in an average annual loss of ecosystem carbon storage of 97.9 ktC/yr. Forests accounted for the largest share of carbon loss at an average rate of 79 ktC/yr, whereas shrublands and grasslands accounted for 0.01 TgC/yr apiece. Expansion of agriculture contributed an additional average annual loss of 0.078 TgC/yr, with 0.057 TgC/yr from forests, 0.009 TgC/yr from shrublands, and 0.012 TgC/yr from grasslands; however this loss was offset owing to higher rates of agricultural contraction. Over the 50-year projection, atmospheric emissions resulting from urbanization and agricultural expansion was estimated at 6.6 TgC with 4.6 TgC coming from forest conversion, 0.9 TgC coming from shrubland conversion, and 1.0 TgC coming from grassland conversion. An additional 2.2 TgC was removed from forest harvest for use in wood products.

Carbon emissions from wildfire averaged 1.4 TgC (0.028 TgC/yr) across the 100 Monte Carlo simulations. However, there was considerable variability, with estimates ranging from 0.001 TgC/yr to 0.108 TgC/yr. Forest fire emissions accounted for approximately 58 percent of wildfire emissions (0.016 TgC/yr), whereas shrubland fire emissions accounted for approximately 23 percent (0.006 TgC/yr);

Table 8.8. Current and projected future total ecosystem carbon storage and percent change in storage by island for the State of Hawai'i.

[TgC, teragrams of carbon; Mean, mean of 100 Monte Carlo iterations; Upper, 97.5 percentile; Lower, 2.5 percentile]

Island	Total ecosystem carbon storage (TgC)				Change in mean total ecosystem carbon storage	
	2011	2061				
		Mean	Upper	Lower	(TgC)	(Percent)
Hawai'i	153.7	165.5	166.7	164.1	11.8	7.7
Kaho'olawe	0.8	0.8	0.9	0.8	0.0	2.9
Kaua'i	28.1	28.6	29.1	28.1	0.6	2.0
Lāna'i	3.0	3.1	3.1	3.0	0.1	4.2
Maui	31.3	32.9	33.2	32.5	1.6	5.0
Moloka'i	8.8	9.3	9.5	9.2	0.5	5.6
O'ahu	27.2	27.3	27.8	26.8	0.2	0.6
Total	252.9	267.6	269.2	265.9	14.7	5.8

Table 8.9. Projected future ecosystem carbon storage by island for the State of Hawai‘i.
[TgC, teragrams of carbon; Mean, mean of 100 Monte Carlo iterations; Upper, 97.5 percentile; Lower, 2.5 percentile]

Island	Living biomass (TgC)				Soil organic carbon (TgC)				Litter and deadwood (TgC)				Total ecosystem carbon storage (TgC)				Change in mean total ecosystem carbon storage	
	2011	2061			2011	2061			2011	2061			2011	2061				
		Mean	Upper	Lower		Mean	Upper	Lower		Mean	Upper	Lower		Mean	Upper	Lower	(Tg)	(percent)
Hawai‘i	31.26	33.162	33.803	32.533	111.887	121.104	121.642	120.619	10.542	11.217	11.396	10.988	153.69	165.484	166.841	164.14	11.794	8
Kaho‘olawe	0.1042	0.1047	0.1147	0.0949	0.66952	0.69393	0.70793	0.6815	0.0382	0.0367	0.0406	0.033	0.81194	0.83536	0.86316	0.80941	0.0234	3
Kaua‘i	6.2592	5.5615	5.7692	5.3645	19.7983	21.28	21.4947	21.0437	2.0141	1.7824	1.8603	1.7203	28.0717	28.6239	29.1242	28.1285	0.5522	2
Lāna‘i	0.3515	0.3719	0.3974	0.35	2.46976	2.5748	2.60255	2.54725	0.14	0.1393	0.1467	0.1295	2.96127	3.08593	3.14657	3.02682	0.1247	4
Maui	6.1069	6.1697	6.3216	5.9923	23.1982	24.6736	24.8496	24.5129	2.0045	2.022	2.0709	1.9538	31.3096	32.8654	33.2422	32.459	1.5558	5
Moloka‘i	1.9409	1.8896	1.9379	1.8214	6.26111	6.81462	6.90595	6.71903	0.6473	0.6431	0.6595	0.6204	8.84925	9.34723	9.50339	9.16079	0.498	6
O‘ahu	5.9432	4.9059	5.097	4.7273	19.3503	20.876	21.1114	20.7162	1.8687	1.5513	1.6198	1.469	27.1622	27.3332	27.8281	26.9125	0.171	1
Total	51.966	52.165	53.069	51.089	183.635	198.017	198.774	197.323	17.255	17.392	17.652	17.131	252.856	267.575	268.824	266.208	15.968	6

Table 8.10. Projected future ecosystem carbon storage by land-cover class for the State of Hawai‘i.
[TgC, teragrams of carbon; Mean, mean of 100 Monte Carlo iterations; Upper, 97.5 percentile; Lower, 2.5 percentile]

Land-cover class	Living biomass (TgC)				Soil organic carbon (TgC)				Litter and deadwood (TgC)				Total ecosystem carbon storage (TgC)				Change in mean total ecosystem carbon storage	
	2011	2061			2011	2061			2011	2061			2011	2061				
		Mean	Upper	Lower		Mean	Upper	Mean		Mean	Upper	Lower		Mean	Upper	Lower	(TgC)	(percent)
Dry forest	26.521	28.739	29.389	28.190	58.889	65.700	66.744	64.591	8.206	9.064	9.254	8.901	93.616	103.503	105.387	101.681	9.887	11
Mesic forest	16.387	11.992	12.471	11.535	26.409	20.901	21.831	19.941	4.900	3.663	3.822	3.515	47.695	36.556	38.125	34.991	-11.139	-23
Wet forest	1.316	2.085	2.205	1.943	4.677	11.784	12.619	10.944	0.405	0.751	0.810	0.695	6.399	14.619	15.634	13.582	8.221	128
Shrubland	2.773	3.518	4.043	2.792	21.636	37.803	45.368	26.068	1.299	1.723	2.001	1.347	25.708	43.044	51.412	30.206	17.336	67
Grassland	0.689	0.481	0.680	0.345	35.901	23.996	35.885	16.127	1.146	0.765	1.092	0.527	37.735	25.241	37.657	16.999	-12.494	-33
Plantation	4.280	4.515	4.797	4.242	4.198	4.589	5.029	4.095	1.299	1.421	1.510	1.323	9.777	10.525	11.336	9.661	0.748	8
Other	---	---	---	---	31.926	33.245	11.299	55.558	---	---	---	---	31.926	33.245	11.299	55.558	1.320	4

emissions from grassland fire accounted for an average of 0.006 TgC/yr. Fire emissions across moisture zones were more evenly distributed than by state-class type; the mesic moisture zone accounted for 0.011 TgC/yr, the dry moisture zone accounted for 0.009 TgC/yr, and the wet moisture zone accounted for 0.008 TgC/yr. Projected emissions for all combinations of state-class type and moisture zone are shown in figure 8.9.

8.4.4. Effects of Major Controlling Processes

The major controlling processes on ecosystem carbon dynamics considered in this assessment include land use and land-use change (for example, urbanization and agricultural expansion and contraction), wildfire, vegetation change (for example, shrub encroachment into grasslands), and the effects of climate change on the composition of moisture zones. In order to understand the relative forcing of each process we conducted a series of sensitivity tests in which each model parameter was omitted from the simulations. We compared estimates of ecosystem carbon stock at the year 2061 for each of the eight resulting alternative scenarios.

Moisture-zone change, shrub encroachment, and agricultural contraction increased ecosystem carbon storage, whereas wildfire, urbanization, and agricultural expansion reduced ecosystem carbon storage (fig. 8.10). Of the model parameters, changes involving land-use transitions had the largest impact on total ecosystem carbon storage. When urbanization was excluded from the model, estimates of ecosystem carbon stock were 4.0–7.4 TgC higher than the BAU scenario. Similarly, when agricultural expansion was excluded, ecosystem carbon stock was estimated to be between 1.5 and 3.5 TgC higher than in the BAU scenario. Compared to land-use changes, wildfire had a small overall impact.

Assumptions about the rate of agricultural contraction had the largest impact on ecosystem carbon estimates. When excluded from the model, ecosystem carbon was projected to be 7.4–10.4 TgC lower than the BAU scenario—roughly equal to the impact of urbanization, agricultural expansion, and wildfire combined. Additionally, the net result of both moisture-zone change and shrub encroachment was an increase in ecosystem carbon storage, with mean departures from the BAU scenario of 1.3 and 0.9 TgC, respectively.

8.5. Key Uncertainties and Limitations

In conducting an assessment such as this, it is important to acknowledge key uncertainties that could have large effects on projection results. Typically, the largest sources of uncertainty when making future projections are associated with projecting changes in complex socioeconomic systems. To overcome this, many studies have used narrative storylines to guide quantification of a wide range of future conditions. Examples of this approach include the IPCC's Special Report on Emission Scenarios (Nakicenovic and Swart, 2000) and the Millennial Assessment (Raskin and others, 2005). However, using these global scenario frameworks can prove challenging at local and regional scales as scenario assumptions may be interpreted in a variety of ways. Various methods of scenario downscaling have been explored, particularly for IPCC SRES scenarios, however no such downscaling was readily available for the State of Hawai‘i. To overcome this limitation, we developed a BAU scenario based on empirically derived measurements of LULC change resulting from urbanization, agricultural expansion and contraction, and wildfire. Historical rates of change were incorporated into the LUCAS model, whereas in each timestep and Monte Carlo simulation the model would sample from the empirical data. For transition types where there was large historical variability (for example, wildfire), the model would project a wide range of future outcomes across the 100 Monte Carlo simulations. However, for some transition types, the historical data revealed temporally consistent trends, which were then carried forward in the scenario projections. This was especially true for trends in agriculture where historical data revealed a consistent net decrease over time. As shown in the sensitivity analysis, assumptions made regarding the rate and trajectory of change in the agricultural sector can have profound impacts on ecosystem carbon storage. As such, future work should consider development of additional scenarios to explore alternative narratives in agricultural expansion and contraction for the State of Hawai‘i.

Forest age is an important model parameter used to control carbon-flux rates within the SF model. However, little is known about the distribution of forest age for the State of Hawai‘i. To overcome this data limitation, we assumed forest age was distributed uniformly across the landscape between 0 and 300 years old, likely an incorrect assumption. Additional work should focus on refining our estimate of forest-age structure, either through plot-based inventories or through known species–biomass relationships. This level of detail was out of the scope of this assessment but should be explored to improve the carbon SF modeling approach.

Future changes in climate can impact ecosystem carbon dynamics in several ways, including increasing and (or) decreasing growth rates owing to changes in temperature, precipitation, and CO_2 fertilization. Because of the geography of the State of Hawai‘i (isolated, small relative area, highly variable topography) there is a general lack of downscaled climate data available for incorporation into studies carried out at the scales and resolution of this assessment. For this research we incorporated projections of changes in moisture zones resulting from climate projections associated with the IPCC SRES A1B scenario. Future efforts should consider expanding the moisture-zone modeling to include new climate scenarios (Representative Concentration Pathways) and climate models (Coupled Model Intercomparison Project, CMIP5) to reflect a range of plausible futures. Additionally, with improved climate-model downscaling for the State of Hawai‘i, alternative projections of temperature, precipitation, and CO_2 concentration could be incorporated into the LUCAS model to reflect changes in NPP which is used to drive the carbon SF model.

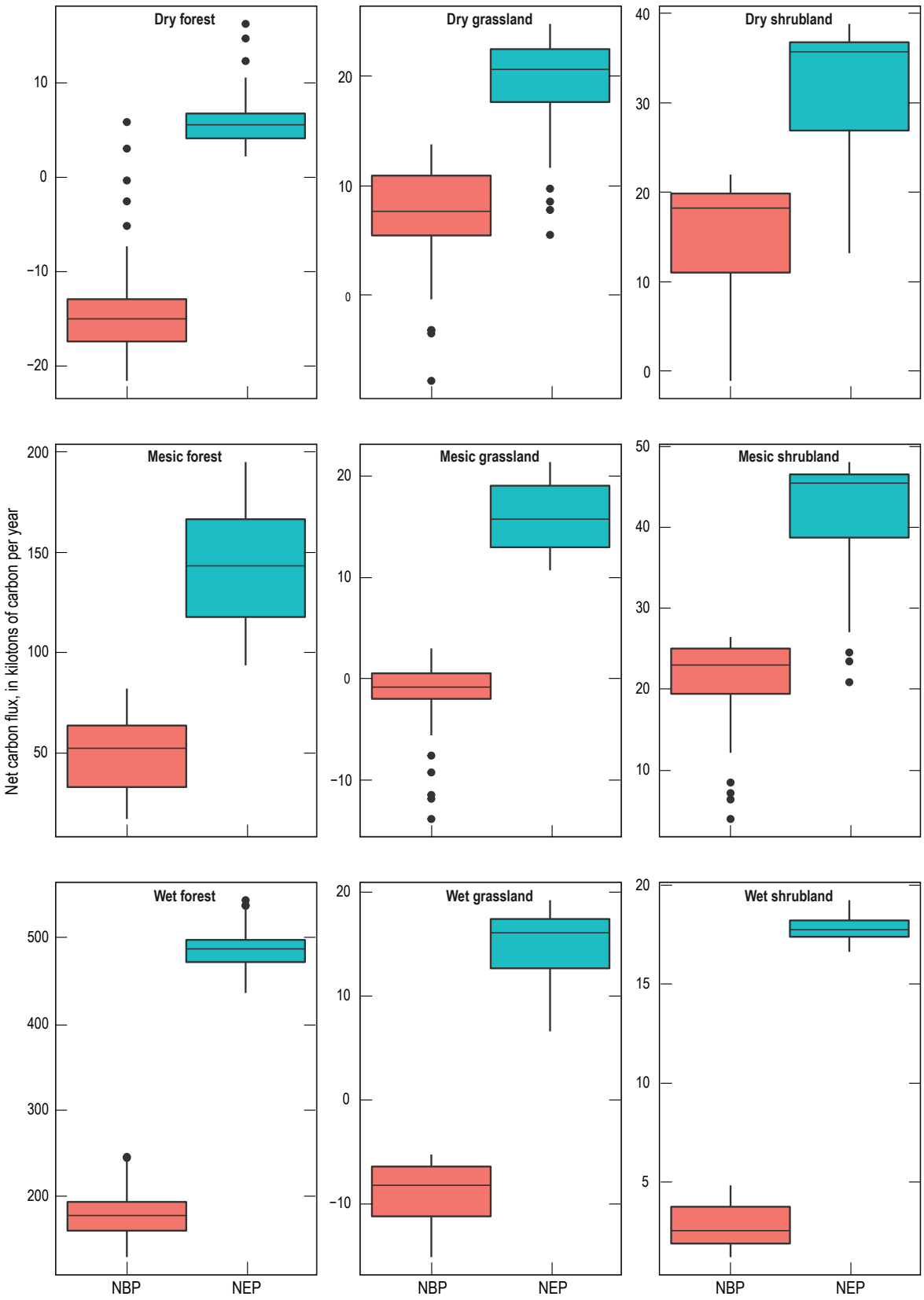

Figure 8.8. Distribution plots of net biome production (NBP) and net ecosystem production (NEP) during the projected future period (2011–2061) for the three major state-class types (forest, shrubland, grassland) and three moisture zones (dry, mesic, wet) considered in this assessment. Boxes represent the 25th and 75th percentile of years and whiskers represent the 10th and 90th percentile of years during the projected future period (2011–2061).

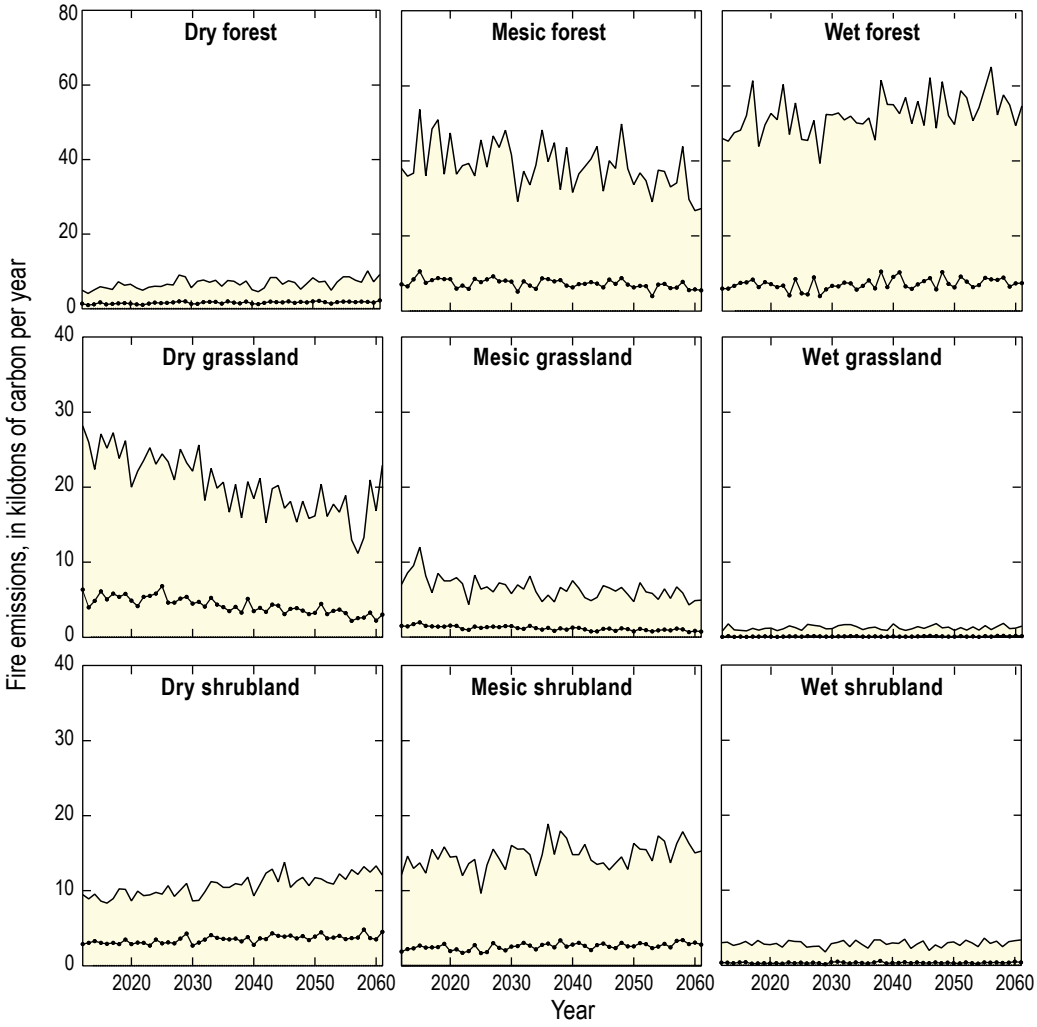

Figure 8.9. Plots of projections of fire emissions across state-class type and moisture zone. The range of values represents the 95-percent confidence interval estimates across 100 Monte Carlo simulations. Dotted black lines show the mean estimates.

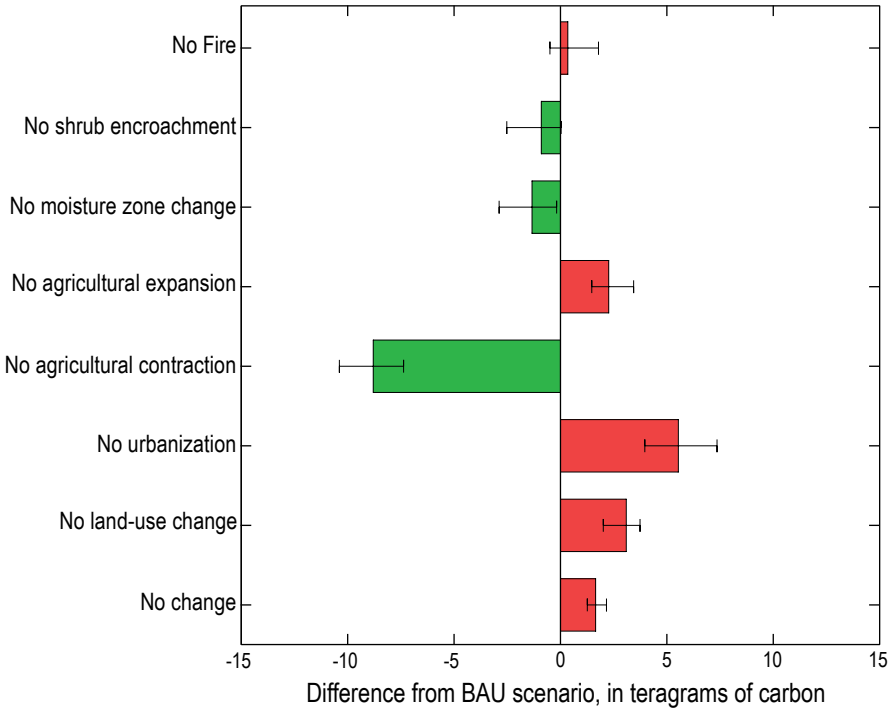

Figure 8.10. Plot of sensitivity analysis of major modeling assumptions. Values are cumulative differences in total ecosystem carbon stock compared to the "business as usual" (BAU) scenario by the year 2061.

Projections of wildfire were based on a sampling protocol using a 10-year time series (2002–2011) from the Monitoring Trends in Burn Severity (MTBS) database. Because of the wide range of variability in the MTBS data, future projections of wildfire represented a wide range of future conditions. However, no long-term trend in wildfire was simulated owing to a lack of either empirically derived relationships of climate and fire or exogenous fire modeling as conducted in the assessment for the conterminous United States. Should additional downscaled climate data become available, alternative wildfire scenarios could be implemented as a means of exploring variability in this important source of terrestrial carbon emissions.

Land-management activities designed to increase terrestrial carbon storage were not explored for this assessment, but can readily be implemented using this modeling framework. Examples may include reforestation, development and utilization of carbon plantations, and biofuel production, among others. Work should be undertaken with local and state-level managers and policy makers to develop alternative land-management scenarios to explore the efficacy of increasing carbon storage and (or) sequestration rates.

8.6. References Cited

Ball, T.J., Woodrow, I.E., Berry, J.A., 1987, A model predicting stomatal conductance and its contribution to the control of photosynthesis under different environmental conditions, chap. 48 *in* Biggins, J., ed., Progress in Photosynthesis Research: Netherlands, Springer, p. 221–224, available at http://dx.doi.org/10.1007/978-94-017-0519-6_48.

Botta, A., Viovy, N., Ciais, P., Friedlingstein, P., Monfray, P., 2000, A global prognostic scheme of leaf onset using satellite data: Global Change Biology, v. 6, no. 7, p. 709–725.

Daniel, C.J., Frid, L., 2012, Predicting landscape vegetation dynamics using state-and-transition simulation models, *in* Proceedings of the first Landscape State-and-Transition Simulation Modeling Conference, Portland, Oreg., June 14–16, 2011: Portland, Oreg., U.S. Department of Agriculture, Forest Service, Pacific Northwest Research Station General Technical Report PNW-GTR-869, 22 p. [Also available at https://www.fs.fed.us/pnw/pubs/pnw_gtr869/pnw_gtr869_002.pdf.]

Daniel, C.J., Frid, L., Sleeter, B.M., Fortin, M.-J., 2016, State-and-transition simulation models—A framework for forecasting landscape dynamics: Methods in Ecology and Evolution, v. 7, no. 11, p. 1413–1423, available at http://dx.doi.org/10.1111/2041-210X.12597.

Eidenshink, J., Schwind, B., Brewer, K., Zhu, Z.-L., Quayle, B., and Howard, S., 2007, A project for monitoring trends in burn severity: Fire Ecology, v. 3, no. 1, p. 3–21.

Farquhar, G.D., von Caemmerer, S., Berry, J.A., 1980, A biogeochemical model of photosynthetic CO_2 assimilation in leaves of C3 species: Planta, v. 149, no. 1, p. 78–90.

Foley, J.A., Prentics, C., Ramankutty, N., Levis, S., Pollard, D., Sitch, S., Haxeltine, A., 1996, An integrated biosphere model of land surface processes, terrestrial carbon balance, and vegetation dynamics: Global Biogeochemical Cycles, v. 10, no. 4, p. 603–628.

Houghton, R.A., Hacker, J.L., and Lawrence, K.T., 1999, The U.S. carbon budget—contributions from land-use change: Science, v. 285, p. 574–578.

Intergovernmental Panel on Climate Change (Paustian, K., Ravindranath, N.H., Amstel, A.), 2006, Volume 4—Agriculture, forestry and other land use, *in* Eggleston, H.S., Buendia, L., Miwa, K., Ngara, T., and Tanabe, K., eds., 2006 IPCC guidelines for national greenhouse gas inventories: Hayama Japan, Institute for Global Environmental Strategies, prepared by the National Greenhouse Gas Inventories Programme, available at http://www.ipcc-nggip.iges.or.jp/public/2006gl/vol4.html.

Kucharik, C.J., Foley, J.A., Delire, C., Fisher, V.A., Coe, M.T., Lenters, J.D., Young-Molling, C., Ramankutty, N., Norman, J.M., Gower, S.T., 2000, Testing the performance of a dynamic global ecosystem model—water balance, carbon balance, and vegetation structure: Global Biogeochemical Cycles, v. 14, no. 3, p. 795–825.

Liu, Z., Wimberly, M., Lamsal, A., Sohl, T., Hawbaker, T., 2015, Climate change and wildfire risk in an expanding wildland–urban interface—a case study from the Colorado Front Range Corridor: Landscape Ecology, v. 30, no. 10, p. 1943–1957, available at http://dx.doi.org/10.1007/s10980-015-0222-4.

Nakicenovic, N., Swart, R., eds., 2000, IPCC Special Report on Emission Scenarios: Cambridge, England, Cambridge University Press, 570 p, available at http://www.ipcc.ch/ipccreports/sres/emission/index.php?idp=0.

National Oceanic and Atmospheric Administration, 2013, Coastal Change Analysis Program (C-CAP) Regional Land Cover Data—Coastal United States: Charleston, S.C., NOAA's Ocean Service, Office for Coastal Management, available at https://coast.noaa.gov/digitalcoast/data/ccapregional/.

Soil Survey Staff, 2015, Gridded Soil Survey Geographic (gSSURGO) Database for Hawaii: United States Department of Agriculture, Natural Resources Conservation Service, accessed August 21, 2015 at https://gdg.sc.egov.usda.gov/ (FY2016 official release).

Osher, L.J., Matson, P.A., Amundson, R., 2003, Effect of land use change on soil carbon in Hawaii: Biogeochemistry, v. 65, no. 2, p. 213–232.

Parton, W.J., Schimel, D.S., Cole, C.V., Ojima, D.S., 1987, Analysis of factors controlling soil organic matter levels, in Great Plains grasslands: Soil Science Society of Americal Journal, v. 51, no. 5, p. 1173–1179.

Parton, W.J., Scurlock, J.M.O., Ojima, D.S., Gilmanov, T.G., Scholes, R.J., Schimel, D.S., Kirchner, T., Menaut, J.C., Seastedt, T., Garcia Moya, E., Kamnalrut, A., Kinyamario, J.I., 1993, Observations and modeling of biomass and soil organic matter dynamics for the grassland biome worldwide: Global Biogeochemical Cycles, v. 7, no. 4, p. 785–809.

Raskin, P., Monks, F., Ribeiro, T., van Vuuren, D., Zurek, M., 2005, Global scenarios in historical perspective, chap. 2 *of* Carpenter, S., Pingali, P., Bennett, E., Zurek, M., eds., Ecosystems and Human Well-Being—Scenarios: Washington, D.C., Island Press, Findings of the Scenarios Working Group, Millennium Ecosystem Assessment Series, p. 35–44.

Sleeter, B.M., Liu, J., Daniel, C., Frid, L., Zhu, Z., 2015, An integrated approach to modeling changes in land use, land cover, and disturbance and their impact on ecosystem carbon dynamics—a case study in the Sierra Nevada Mountains of California: AIMS Environmental Science, v. 2, no. 3, p. 577–606, available at http://dx.doi.org/10.3934/environsci.2015.3.577.

Verberne, E., Hassink, J., De Willigen, P., Groot, J., Van Veen, J., 1990, Modeling organic matter dynamics in different soils: Netherlands Journal of Agricultural Science, v. 38, no. 3, p. 221–238.